

The Carina Project: I. Bright Variable Stars¹

M. Dall’Ora^{1,2,3}, V. Ripepi¹, F. Caputo², V. Castellani^{2,4}, G. Bono², H. A. Smith⁵, E. Brocato⁶, R. Buonanno^{2,3}, M. Castellani², C. E. Corsi², M. Marconi¹, M. Monelli^{2,3}, M. Nonino⁷, L. Pulone², A. R. Walker⁸

1. INAF - Osservatorio Astronomico di Capodimonte, Via Moiariello 16, 80131 Napoli, Italy; dallora, ripepi@na.astro.it
2. INAF - Osservatorio Astronomico di Roma, Via Frascati 33, 00040 Monte Porzio Catone, Italy; bono, buonanno, caputo, corsi, dallora, mkast, monelli, pulone, vittorio@mporzio.astro.it
3. Università Tor Vergata, Via della Ricerca Scientifica 1, 00133 Rome, Italy
4. INFN - Sezione di Ferrara, via Paradiso 12, 44100 Ferrara, Italy.
5. Dept. of Physics and Astronomy, Michigan State University, East Lansing, MI 48824, USA; smith@pa.msu.edu
6. INAF - Osservatorio Astronomico di Collurania, Via M. Maggini, 64100 Teramo, Italy; brocato@te.astro.it
7. INAF - Osservatorio Astronomico di Trieste, Via G.B. Tiepolo 11, 40131 Trieste, Italy; nonino@ts.astro.it
8. Cerro Tololo Inter-American Observatory, National Optical Astronomy Observatories, Casilla 603, La Serena, Chile; awalker@noao.edu

¹Based on observations collected at the European Southern Observatory, La Silla, Chile on Osservatorio Astronomico di Capodimonte guaranteed time.

ABSTRACT

We present new BV time series data of the Carina dwarf spheroidal (dSph) galaxy. Current data cover an area of ≈ 0.3 degree² around the center of the galaxy and allowed us to identify 92 variables. Among them 75 are RR Lyrae stars, 15 are "bona fide" Anomalous Cepheids, one might be a Galactic field RR Lyrae, and one is located along the Carina Red Giant Branch (RGB). Expanding upon the seminal photographic investigation by Saha, Monet, & Seitzer (1986) we supply for the first time accurate estimates of their pulsation parameters (periods, amplitudes, mean magnitude and colors) on the basis of CCD photometry. Approximately 50% of both RR Lyrae and Anomalous Cepheids are new identifications. Among the RR Lyrae sample 6 objects are new candidate double-mode (*RRd*) variables. On the basis of their pulsation properties we estimated that two variables (V152, V182) are about 50% more massive than typical RR Lyrae stars, while the bulk of the Anomalous Cepheids are roughly a factor of two more massive than fundamental mode (*RRab*) RR Lyrae stars. This finding supports the evidence that these objects are intermediate-mass stars during central He burning phases.

We adopted three different approaches to estimate the Carina distance modulus, namely the First Overtone Blue Edge (FOBE) method, the Period-Luminosity-Amplitude (*PLA*) relation, and the Period-Luminosity-Color (PLC) relation. We found $DM = 20.19 \pm 0.12$, a result that agrees quite well with similar estimates based on different distance indicators.

The data for Carina, together with data available in the literature, strongly support the conclusion that dSph galaxies can barely be classified into the classical Oosterhoff dichotomy. The mean period of *RRab* in Carina resembles that found for Oosterhoff type II clusters, whereas the ratio between first overtones (*RRc*) and total number of RR Lyrae is quite similar to that found in Oosterhoff type I clusters.

Subject headings: galaxies: dwarf – galaxies: individual: (Carina) – galaxies: Local Group – stars: distances – stars: horizontal branch – stars: oscillations

1. Introduction

As suggested in several recent studies, and extensively reviewed by Mateo (1998, hereinafter M98) and van den Bergh (1999, hereinafter VDB), dSph galaxies are the most common type of galaxies in the Local Group (LG), and presumably in the present-day Universe. Therefore, they are as cornerstones on the path to understanding several aspects of galaxy evolution. They are metal-poor systems (M98, VDB), with a metal content, $Z < 0.001$, that resembles the metallicity of Galactic Globular Clusters (GGCs). On the other hand, only a few of them, namely Tucana (Lavery et al. 1996; Castellani et al. 1996) and possibly Ursa Minor (Carrera et al. 2002; Ikuta & Arimoto 2002) and Draco (Dolphin 2002), host a *single* stellar population older than ≈ 10 Gyr that might be coeval to GGCs. As a whole, dSphs are composite systems which are characterized by a sizable intermediate-age (4-8 Gyr) stellar component (VDB 1999), and show compelling evidence of multiple star-formation episodes that range from ~ 12 -14 Gyr to very recent epochs ~ 2 -3 Gyr. Although it was at first suggested that star formation in the Leo I dwarf spheroidal began only ~ 7 Gyr ago, it is now known that, like the other dwarf spheroidals, it contains an underlying ancient stellar population (Caputo et al. 1999; Gallart et al. 1999; Held et al. 2000, 2001). Empirical facts above discussed indicate that the old stellar populations in LG dSphs are approximately coeval with GGCs (Da Costa 1999). At the same time, current data also suggest that these systems retained substantial amount of gas for a significant fraction of the Hubble time. In fact, current photometric surveys support the evidence that dSphs experienced star formation episodes that lasted several Gyrs. Moreover and even more importantly, in several dSphs the most recent star formation episodes date back a few Gyr ago. This circumstantial evidence is at odds with current theoretical predictions concerning the formation and evolution of LG dSph (see Moore et al. 1999 and Monelli et al. 2002, hereinafter Paper II).

In the dSph realm, the Carina dSph is one of the the most prominent examples of multiple stellar populations, since its Color-Magnitude Diagram (CMD) shows a surprisingly complex star-formation history. On the basis of the comparison between the multiple Main Sequence Turn Off and theoretical isochrones, it has been suggested that this galaxy underwent significant bursts of star formation at 3, 7, and 15 Gyr ago (Hurley-Keller, Mateo, & Nemeč 1998; Smecker-Hane et al. 1996; Paper II). Moreover, Smecker-Hane et al. (1994) showed that two morphologically distinct Horizontal Branch (HB) structures are present: the former ("old") has a visual magnitude $V \sim 20.65$ mag at the RR Lyrae gap and extends to bluer colors, the latter ("young") is located close to the RGB and it is ~ 0.25 mag brighter than the old one. Interestingly, the periods of the RR Lyrae stars in Carina (Saha, Monet & Seitzer 1986; hereinafter SMS) suggest that this galaxy, like most dSph galaxies, such as Draco (Baade & Swope 1961), is a 'bridge' between Oosterhoff type

I (OoI) and type II (OoII) clusters.

The Carina Project was driven by these stimulating peculiarities and aims at fully exploiting modern technological capabilities of wide field imagers to improve current knowledge on the stellar content of dSph galaxies in the LG. In this context it is worth mentioning that Carina is a fundamental laboratory, since it is relatively close and the CMD can allow us to supply a complete census of its stellar content on a star-by-star basis from the tip of the RGB down to the Turn-Off of the old population. At the same time, Carina is also a fundamental laboratory to provide new insights on the properties of variable stars such as Anomalous Cepheids (Bono et al. 1997a), RR Lyrae stars (SMS), and dwarf Cepheids (Mateo et al. 1998). Moreover, detailed information on static and variable stars will supply tight constraints on the evolutionary history of Carina.

Based on a series of exposures collected with the Wide Field Imager (WFI) available at the 2.2m ESO/MPI telescope (La Silla, Chile), we determined B and V magnitudes for $\sim 68,000$ stars, extending from the tip of the RGB ($V \sim 17.5$ mag) down to $V \sim 25.5$ mag. Photometric data of the observed static stars are discussed in a companion paper (Paper II), while the present investigation deals with the bright pulsating variables, namely RR Lyrae and Anomalous Cepheids. The seminal work in this field was the SMS survey and no later extensive investigation appeared in the literature during the last decade. The SMS study reported the discovery of 172 candidate variables in the central region of Carina and the search was based on photographic B plates taken at the prime focus of the CTIO 4m telescope. The area covered was 1 degree^2 centered on the bright field star SAO 234657, which is located very close to the Carina center. Light curves and periods were obtained for 58 out of the 73 variables identified as RR Lyrae members of the Carina galaxy. RR Lyrae variables are considered "bona fide" tracers of ancient stellar populations, therefore the presence of large numbers of RR Lyrae provided the first evidence that an underlying old population was present in this galaxy. However, the mean period of $RRab$ stars derived by SMS is ~ 0.62 days, which is intermediate between that of OoI (~ 0.55 days) and OoII (~ 0.65 days) clusters. This suggests that the evolutionary history of the old stellar population in Carina might be different than that of GGCs.

Among the remaining 15 objects identified as variables by SMS, 8 showed RR Lyrae-like light curves but magnitudes significantly brighter than $B=21.10$ mag, the mean B magnitude of RR Lyrae stars. Later studies (Da Costa 1988; Nemec, Nemec, & Lutz 1994, and references therein) suggested that they are Anomalous Cepheids. These variables are intrinsically brighter than RR Lyrae stars and follow a Period-Luminosity (PL) relation with the less luminous ones (~ 0.5 mag above the RR Lyrae level) having shorter periods ($P \sim 0.3$ day) and the most luminous ones (~ 2 mag brighter than RR Lyrae stars) longer

periods ($P \sim 2$ day). Concerning their evolutionary status, there is a general consensus that they are metal-poor central He-burning structures with mass larger than $1.3M_{\odot}$, but their origin (single young stars or old merged binary systems) is still debated (see Bono et al. 1997a, and references therein). In any case, they are almost absent in GGCs (except one in NGC 5466 and two suspected candidates in ω Centauri), whereas they have been found in *all* dSphs that have been searched for variable stars. The presence of these variables might be taken as indicative of an underlying intermediate-age population or at least of the presence of a significant Blue Straggler component. The reader interested in a more detailed discussion is referred to paper II.

Together with these straightforward considerations, we note that the radial pulsation phenomenon provides two relevant observables, period and luminosity amplitude, that are tightly connected with the stellar mass, luminosity, and effective temperature of the pulsators (see Bono et al. 1997b; Caputo, Degl’Innocenti, & Marconi 2002, and references therein). These observables are affected neither by interstellar reddening nor by distance and represent a unique opportunity for testing the prescriptions of evolutionary and pulsation theories. In summary, pulsation periods and amplitudes together with magnitudes and colors, are the benchmarks to unambiguously constrain the structural parameters of variable stars, and to provide useful clues to understand the star-formation history of the host galaxy.

This paper is organized as follows: the next section addresses the identification of the Carina variables, while the new estimates of periods and mean magnitudes are presented in §3. Evaluations of the Carina distance modulus, based on the properties of RR Lyrae stars, are discussed in §4. A brief summary closes the paper.

2. Identification of variables

Observations were collected by two of us (E.B. and V.C.) over three consecutive nights (January 5-7, 2000) at the 2.2m ESO/MPI telescope (La Silla, Chile) equipped with the WFI which is a mosaic camera with 8 EEV 2046x4098 chips. The pixel scale is 0.238 arcsec/pixel and the total field of view is $\approx 34 \times 33$ arcmin, including gaps between CCDs whose width is 23.8 and 14.3 arcsec along right ascension and declination, respectively. We observed with the *BV* filters, using consecutive exposures of ~ 500 s each in order to secure a good sampling of the light curve over the pulsation cycle. In total we obtained 54 *BV* pairs during the three nights. The log of the observations is presented in Paper II together with details concerning the seeing, the absolute, and the relative calibration, as well as the reduction strategy.

The main aim of this investigation is to identify bright variable stars in Carina and to estimate their pulsation parameters. To accomplish this project we decided to perform aperture photometry and the reason for this choice is twofold. *i)* The field covered by our data is only marginally affected by crowding, even in the innermost regions (see the identification maps in appendix A). *ii)* Exposure times were chosen to perform accurate photometry on individual frames at the luminosity typical of old HB stars, namely $V \approx 20.7$, $B \approx 21.0$. Data were collected with an average seeing better than 1 arcsec both in the B and in the V band. Therefore the photometry was performed using in the two bands a radius of four pixels. Fig. 1 shows the standard deviation as a function of the instrumental magnitude for the chip # 51 of the frames # 46388 (*b*) and # 46391 (*v*) (see Table 2 in Paper II). Data plotted in this figure show that the photometric accuracy for an RR Lyrae variable at minimum light, i.e. $b \approx 15.4 - 15.8$ (corresponding to $B \approx 21.3 - 21.7$) and $v \approx 15.3 - 15.7$ (Corresponding to $V \approx 21.0 - 21.4$), is on average equal to 0.02 mag. Note that current uncertainties do not account for calibration errors.

The search for variable stars was carried out using the Welch & Stetson (1993) algorithm. This method correlates the magnitude variations in two or more photometric bands, and estimates a variability index I that is very robust against spurious effects. The higher the value of I , the higher is the probability that the star is actually a "bona fide" variable star. We checked all the stars with $I \geq 10$ and we found that the majority of variable candidates were characterized by $I \geq 50$. Note that the adopted aperture photometry did not detect very faint variable stars ($V \geq 22$ mag) and/or those characterized by very small luminosity amplitudes. For this reason, we plan to perform psf photometry on current data as well as on an additional set of BV time series data collected by one of us (A.W.) with the Mosaic Imager available at the CTIO Blanco 4m telescope.

A period search was carried out on the suspected variables by means of a Fourier analysis. The accuracy of period evaluations depends on the period itself and on the time interval covered by observations (three nights), and it ranges from 0.004 to 0.04 days. The phased light curves were fitted using cubic splines. Eventually, amplitudes and mean magnitudes (intensity-averaged and magnitude-averaged) were obtained by integrating the fitted light curves. Table 1² summarizes the results. The first column gives the identification number according to SMS, while for the new detected variables the SMS running number was continued, from 173 to 207. The columns 2 and 3 give $\alpha(2000)$ and $\delta(2000)$ coordinates, while the last two columns list SMS and current individual notes. Inspection of the data in Table 1 shows that all the variables found by SMS in the field covered by the present study,

²The complete version of this table is only available in the on-line edition of the manuscript.

and for which light curves and periods were obtained by those authors, have been recovered, with the exception of 7 objects, namely V8, V9, V12, V28, V38, V62, and V69. The distribution of these unrecovered variables in the Bailey diagram (luminosity amplitude vs period) according to SMS data is somehow peculiar, since they present very short periods, 0.06 - 0.26 days, but B amplitudes, 0.77 - 1.44 mag, typical of $RRab$ variables. According to our data they do not seem to be variable stars, and therefore 52 out of the 57 objects tagged as variables by SMS are confirmed to be variables. At the same time, only 5 out of the 81 objects identified by SMS as suspected variables, i.e. without light curves and periods, have been identified as variables, namely V87, V138, V141, V142, and V151. The candidate variable V161, is still a suspected variable.

On the other hand, 35 new variables have been identified. This means that we end up with a total number of 92 detected variables. The individual B,V measurements for the entire sample of variables are listed in Table 2³ For each variable the first three columns give the Heliocentric Julian day, the B magnitude, and the photometric error. The columns 4,5, and 6 list the same data but for the V-band measurements. The current sample of variable stars includes 6 suspected double-mode pulsators (V11, V26, V84, V89, V192, V198, and V207). Note that 4 of them are in the SMS list, but they were classified as $RRab$ (V26, V84 V89) or RRc (V11) variables. To firmly assess the variability of the 7 SMS variables that did not match our variability criterion, as well as to properly classify the suspected multi-mode variables, new data that cover a longer time interval are required.

3. Periods, amplitudes, and mean values

Table 3 lists from left to right identification, classification, epoch, period (days), logarithmic period, magnitude-averaged [$\langle V \rangle$, $\langle B \rangle$], as well as intensity-averaged [$\langle V \rangle$, $\langle B \rangle$] magnitudes and color [$\langle B \rangle - \langle V \rangle$], V and B amplitudes (A_V , A_B) for the 92 variables identified in the current photometric survey. Variable classification (ab= $RRab$; c= RRc , d= RRd , AC=Anomalous Cepheid) relies on these observables and it was a straightforward procedure, since different groups of radial variables do obey well-established relations among luminosity, temperature, period, and luminosity amplitude (see later). Note that for candidate double-mode variables and for poorly-sampled light curves current estimates of pulsation parameters are less accurate. The periods of these objects are listed in italic and the pulsation parameters are given with two decimal figures. Fig. 2a-2l show the light curves of current variables. In particular Fig. 2a-2h display variables fainter than

³The complete version of this table is only available in the on-line edition of the manuscript.

$\langle V \rangle = 20$ mag, Fig. 2i the suspected double-mode pulsators, Fig. 2j-2k the variables brighter than $\langle V \rangle = 20$ mag, and Fig. 2l the variables V173 and V194. The error bar plotted in the top left panel of Fig. 2a shows the typical B,V photometric uncertainty for an RR Lyrae star at minimum light. Fig. 3 shows the location of the Carina variables in the Color-Magnitude diagram, derived in Paper II, according to their $\langle V \rangle$ magnitudes and $\langle B \rangle - \langle V \rangle$ colors. One can easily recognize "old" HB stars extending from the flat RR Lyrae region ($V \sim 20.7$ mag) to bluer colors, and the "intermediate-age", stubby red clump stars located at $V \sim 20.5$ mag and $B - V \sim 0.7$ mag. The variables are plotted with different symbols, according to their position in the CMD. Specifically, the red variable V173 located close to the Carina RGB is marked with a cross, while the very bright RR Lyrae V194, probably belonging to the Galactic field, with a square. The remaining 90 variables are plotted using circles and triangles, depending on whether the apparent mean visual magnitude is fainter or brighter than $\langle V \rangle = 20$ mag.

Fig. 4 shows a zoom of the instability strip in the Carina CMD. The symbols are the same as in Fig. 3, but variables with poorly-sampled light curves, uncertain periods, and possible photometric blends are displayed with open symbols. Moreover, for the sake of the discussion, we identify the two variables, V158 and V182, in the "faint" group that appear significantly brighter than the mean intensity-averaged magnitude, $\langle V \rangle_m = 20.68 \pm 0.06$ mag (solid line), of Carina RR Lyrae. A glance at the distribution of the variables plotted with circles, and accounting for a reddening $E(B - V) = 0.03 \pm 0.02$ mag (see M98 and Paper II), shows that they behave as typical globular cluster RR Lyrae stars, i.e. variables located in the flat region of the HB with intrinsic $B - V$ colors in the range $0.15 - 0.4$ mag (see, e.g., the extensive survey of RR Lyrae stars in M3 by Corwin & Carney 2001).

The top panel in Fig. 5 shows the same variables plotted in the visual magnitude $\langle V \rangle$ versus $\log P$ plane (Bailey diagram). Among the variables fainter than $\langle V \rangle = 20$ mag, one clearly identifies the period gap expected between first-overtone (RRc) and fundamental ($RRab$) variables. On this basis, variables with $\log P \leq -0.35$ and $\log P \geq -0.25$ should be c -type (squares) and ab -type (dots) RR Lyrae, respectively. In this figure, the short-period variables which are suspected to be double-mode pulsators are marked with an asterisk. As already found in previous studies (M15, Bingham et al. 1984; IC4499, Walker & Nemeč 1996; Draco, Nemeč 1985), they are located around the long-period edge of the RRc period distribution. As far as bright variables are concerned, they show periods and colors similar to RR Lyrae. However, their luminosity when compared with the luminosity of RR Lyrae becomes, on average, brighter and brighter toward longer periods. Bearing in mind that the luminosity increases toward bluer colors (see Fig. 4), one can recognize among these bright variables the behavior of massive ($\geq 1.3M_\odot$), He-burning, metal-poor pulsators discussed by Bono et al. (1997a). According to this circumstantial evidence, the variables brighter

than $\langle V \rangle = 20$ mag might be tentatively classified as Anomalous Cepheids. Data plotted in the top panel of Fig. 5 indicate that the Anomalous Cepheids can be divided into two period-luminosity relations, perhaps signifying different pulsation modes as suggested by empirical (Nemec et al. 1994; Pritzl et al. 2002) and theoretical (Bono et al. 1997a) evidence. Note that according to this selection criterium the two variables V158 and V182 appear to be evolved RR Lyrae stars, since they present (B-V) colors quite similar to V149, the faintest AC, but their periods are significantly longer (see *infra*).

The visual amplitude A_V versus $\log P$ diagram of the variables fainter than $\langle V \rangle = 20$ mag is presented in the bottom panel of Fig. 5. Data plotted in this panel show that the previous classification is confirmed. The *RRab* candidates display a well-defined anti-correlation between A_V and period, and indeed they attain larger amplitudes in the short-period range. On the other hand, the amplitude of *RRc* candidates increases in the short-period ranges and decreases toward longer periods. It is worth noting that the almost linear amplitude-period correlation of *ab*-type variables and the characteristic "bell-shape" behavior of *RRc* variables are fully predicted by nonlinear pulsation models. According to Bono et al. (1997b), the amplitude of fundamental pulsators increases from the red edge (long-period) towards the blue edge (short-period) of the fundamental instability strip, whereas for first overtone pulsators the amplitude attains vanishing values close to the red and the blue edge of its unstable region, and reach the maximum amplitude in the middle of the first overtone instability strip.

In the following we will try to estimate the mass range covered by the Carina variables, based on the observed quantities inferred by high-quality light curves and using the constraints from pulsation theory. It is well known that the pulsation period depends on the structural parameters (mass, luminosity, and effective temperature) of the variable. During the last few decades the analytical relation provided by van Albada & Baker (1971) based on linear fundamental (F) pulsation models

$$\log P_F = 11.497 + 0.84 \log L/L_\odot - 0.68 \log M/M_\odot - 3.48 \log T_e \quad (1)$$

has been the crossroad of several investigations focused on the evolutionary status of RR Lyrae stars. After that pioneering approach to radial pulsation, extensive grids of nonlinear, nonlocal, and time-dependent convective models have been computed (Bono et al. 1997b; Caputo et al. 2000; Bono et al. 2001; Bono et al. 2002; Di Criscienzo, Marconi, & Caputo 2002, hereinafter DMC) for wide ranges of metal content ($Z = 0.0001 - 0.02$), stellar mass ($M/M_\odot = 0.53 - 0.80$) and luminosity ($\log L/L_\odot = 1.5 - 1.9$). The new theoretical scenario provides not only periods and modal stability across the blue edge but also the variation of bolometric luminosity along the pulsation cycle. Once the bolometric

light curves are transformed into the observational plane using bolometric corrections and color-temperature relations predicted by atmosphere models (Castelli, Gratton, & Kurucz 1997a,b), the nonlinear models predict observables such as amplitudes, mean magnitudes, colors and the modal stability across the red edge. This means that the pulsation relation [eq. (1)] can be given in terms of observables, namely the mean magnitude instead of luminosity, and the amplitude or the mean color instead of the effective temperature.

Fig. 6 shows, according to DMC computations, the period-amplitude diagram of selected fundamental pulsators with the labeled mass, luminosity and metal content. Together with the well-established, and observationally confirmed, increase of the visual amplitude A_V toward shorter periods⁴, one finds a dependence on both stellar luminosity (top panel) and mass (bottom panel). Specifically, for stellar masses ranging from 0.65 to $0.80M_\odot$ and metal abundances from 0.0001 to 0.001, and by adopting intensity-averaged magnitudes, DMC computations of fundamental models supply the following Period-Luminosity-Amplitude (*PLA*) relation

$$\log P_F = 0.080(\pm 0.02) - 0.396 < M_V > - 0.593 \log M/M_\odot - 0.167 A_V \quad (2)$$

It is noteworthy that the constant term and the coefficient of the V amplitude do depend on the adopted mixing length parameter $l/H_p=1.5$. The effect of convection in the external layers of stellar envelopes is to quench pulsation driving, therefore a variation of l/H_p causes a change in the effective temperature width of the instability region. The red edge of the instability strip, i.e. in the region of *ab*-type variables are located, is more sensitive to the adopted mixing length than the blue edge (Bono, Castellani, & Marconi 2002). However, let us now account for a sample of *RRab* stars located at the same distance, but with different absolute magnitudes and stellar masses. Since the period variation due to a spread in the luminosity of individual variables can be easily removed by adopting the "reduced" period, i.e. $\log P'_F = \log P_F + 0.396(< V > - < V >_m)$ at the averaged observed magnitude $< V >_m$, the "reduced" Bailey diagram should give information on the spread in mass of individual variables. For example, by adopting a mass range of $M = 0.65 - 0.80M/M_\odot$, the expected dispersion in the "reduced" period, at constant A_V , is $\Delta \log P'_F \sim 0.09$.

Fig. 7 shows the A_V versus $\log P'_F$ diagram for the Carina *RRab* stars, together with

⁴Note that, DMC models confirm previous findings concerning the pulsation properties close to the "intersection point" between first-overtone and fundamental blue edges (Bono, Caputo, & Stellingwerf 1995; Bono et al. 1997b). Above this limit fundamental amplitudes present a "bell-shaped" distribution, i.e. the amplitude is vanishing either close to the blue and to the red edge of the instability region.

similar diagrams for variables in M3 ($\langle V \rangle_m = 15.62$ mag, Corwin & Carney 2001) and M15 ($\langle V \rangle_m = 15.82$ mag, Bingham et al. 1984). We selected these two clusters because they host sizable samples of RR Lyrae stars (207 in M3, 88 in M15) for which accurate pulsation parameters are available, and they are the typical OoI (M3) and OoII (M15) Galactic prototypes. Moreover, they bracket the Carina mean metallicity, i.e. $[\text{Fe}/\text{H}] = -1.7$ (see Paper II), while the mean metallicity for M3 and M15 are $[\text{Fe}/\text{H}] = -1.3$, and -2.15 (Harris 1996), respectively. The dashed lines plotted in Fig. 7 show a period dispersion at constant amplitude of $\Delta \log P'_F = 0.09$, as estimated using eq. (2) and by assuming a mass range of $M = 0.65 - 0.80 M_\odot$. It is noteworthy that all the variables in the three stellar systems fulfill this assumption, with the exception of V158 and V182 in Carina which appear to have a significantly shorter reduced period. According to eq. (2), we estimate that their mass is larger by $\sim 50\%$ than the bulk of Carina *RRab* variables.

A further observable which is related to the effective temperature is obviously the $B - V$ color. Note that the observed color is not the static color, i.e. the color of the variable if it were a static star. Several empirical investigations and the data listed in Table 3 show that the magnitude-averaged colors ($B - V$) are redder than the intensity-averaged colors ($\langle B \rangle - \langle V \rangle$). This difference for *RRab* stars increases when moving from low (long period) to high-amplitude (short period) pulsators. Nonlinear pulsation models (Bono, Caputo & Stellingwerf 1995; DMC) confirm such a behavior, and also provide the amplitude-correction to observed mean colors to estimate the intrinsic static ($B - V$)_s color. Given the typical distribution of RR Lyrae variables in the period-amplitude diagram, one clearly understands that this correction for *RRc* is quite small, whereas for the shorter period *RRab* variables it becomes a sizable correction. In particular, for $(B - V)_s = 0.27$ mag and $A_V \sim 1.5$ mag, one finds $\langle B \rangle - \langle V \rangle \approx 0.24$ mag and $(B - V) \approx 0.31$ mag. Note also that the mean V magnitudes are always fainter than the static value V_s , again with the difference increasing with A_V . With $A_V \sim 1.5$, one has $V_s - \langle V \rangle \sim -0.14$ mag and $V_s - \langle V \rangle \sim -0.04$ mag. As a consequence, in the region of the instability strip where the transition between the two pulsation modes takes place, *RRc* and *RRab* variables with similar parameters (mass, luminosity, and effective temperature) may have significantly different mean magnitudes and colors. Once the photometric database of this project will be completed we plan to derive static magnitudes and colors for all the Carina variables and to perform a detailed analysis. At present, since the nonlinear pulsation models provide directly information on the mean magnitudes, from DMC computations with $0.0001 < Z < 0.001$ we derive the following Period-Luminosity-Color (*PLC*) relation

$$\log P_F = -0.553(\pm 0.014) - 0.617 \log M/M_\odot - 0.347 \langle M_V \rangle + (1.007 - 0.070 \log Z)[\langle B \rangle - \langle V \rangle] \quad (3)$$

This equation also accounts for first overtone pulsators, provided that the period has been "fundamentalized", i.e. $\log P_F = \log P_{FO} + 0.13$. According to this equation, a homogeneously reddened sample of RR Lyrae stars located at the same distance and with roughly constant mass and metallicity, but different luminosity and color, should have a well-established locus in the $\log P'_F (= \log P_F + 0.347(\langle V \rangle - \langle V \rangle_m))$ versus $\langle B \rangle - \langle V \rangle$ plane. On the contrary, if the stellar mass of RR Lyrae stars is significantly different, then the more massive variables should present, at fixed color, shorter reduced periods, and vice versa.

Fig. 8 shows the reduced periods versus dereddened color for RR Lyrae stars in Carina, M3 and M15. Also in this case, the dashed lines depict the predicted period dispersion at constant color ($\Delta \log P'_F \sim 0.09$) by assuming the mass range of $M = 0.65 - 0.80 M_\odot$. Data plotted in this figure show that all the variables in M3 and M15 are quite consistent with the adopted mass range, whereas the RR Lyrae stars in Carina seem to suggest a slightly larger range. This hypothesis will be checked using static values. In any case, present data plotted in Fig. 8 confirm that V158 and V182 are significantly more massive (by $\sim 50\%$) than the bulk of Carina RR Lyrae stars.

We can now take into account the variables brighter than $\langle V \rangle = 20$ mag. Fig. 9 shows the comparison between variables with good-quality light curves and the mean locus of RR Lyrae stars plotted in Fig. 8 (dashed line). Data plotted in this figure disclose that their reduced periods are shorter than those of V158 and V182, thus suggesting even larger masses. As a whole, the Carina bright variables attain reduced periods that are systematically shorter than the predicted values $\Delta \log P'_F = -0.11$ and -0.25 (solid lines) provided by eq. (3) with mass values that are 1.5 and 2.5 times larger than the bulk of fundamental variables fainter than $\langle V \rangle = 20$ mag. Note that similar mass estimates for ACs have been derived in Paper II on the basis of the comparison between Zero Age He-burning structures and empirical data. However, since previous studies (Nemec, Nemec, & Lutz 1994; Bono et al. 1997a) have suggested the presence in dSphs of both fundamental and first overtone Anomalous Cepheids, a more detailed analysis is required to constrain the pulsation mode, and in turn to estimate the individual mass of these variables.

Finally, let us compare the pulsation properties of "bona fide" Carina RR Lyrae stars (with the exception of V158 and V182) with variables observed in other dSph galaxies and globular clusters in the Milky Way. According to the data listed in Table 3, we derived $\langle \log P_{ab} \rangle = -0.200$ ($\langle P_{ab} \rangle = 0.631$ days) and $N_{cd}/(N_{ab} + N_{cd}) = 0.29$, where N_{cd} includes the suspected *RRd* variables. where N_{ab} is the number of *RRab* variables as well as N_{cd} the number of *RRc* and suspected *RRd* variables. Data plotted in Fig. 10 disclose that, the mean period of *RRab* variables in Carina (filled triangle) appear quite

similar to the values observed in RR Lyrae-rich OoII clusters (filled circles), whereas the fraction of *RRc* is significantly smaller when compared with those clusters and close to the values observed in OoI systems (open circles). Current data for RR Lyrae in dSphs (open triangles, see also Table 4), confirm that these stellar systems can be hardly classified into the "classical" Oosterhoff groups. In fact, Ursa Minor presents a mean fundamental period ($\log \langle P_{ab} \rangle = -0.197$) and a fraction of *RRc* stars ≈ 0.4 , that are typical of Oo type II clusters, while Sagittarius has $\log \langle P_{ab} \rangle = -0.241$ and a fraction of *RRc* stars ≈ 0.2 , that are typical of Oo type I clusters. Moreover, Fig. 11 shows the comparison between the period distribution of *RRab* stars in Carina with the cumulative period distribution of three OoII clusters with sizable samples of RR Lyrae, namely M15 (Cox, Hodson, & Clancy 1983; Silbermann, & Smith 1995), M53 (Kopacki 2000), and M68 (Walker 1994). For these clusters current data suggest $N_{ab}=49$, $\log P_{ab} \geq -0.187$ ($\langle P_{ab} \rangle = 0.653$ days), and $N_{cd}/(N_{ab} + N_{cd}) \sim 0.50$. Interestingly enough, the Carina variables show a gaussian distribution with a peak near $\log P \sim -0.20$, whereas the cluster variables show a bimodal distribution with a long-period peak at ~ -0.14 . Whether this difference might be due to the fact that Carina shows a redder HB morphology than OoII clusters it is not clear. However, this might mean that Carina lacks of significant numbers of bright variables evolving redward from the blue side of the RR Lyrae instability strip (Caputo, Tornambé & Castellani 1989). Note that this working hypothesis could explain the low fraction of *RRc* variables detected in Carina.

4. RR Lyrae stars as distance indicators

RR Lyrae stars have been one of the most popular distance indicator for metal-poor stellar systems, since their intrinsic luminosity is expected to mainly depend on the metal content $[\text{Fe}/\text{H}]$. As a consequence, in the last few decades many investigations have been devoted to the slope and the zero-point of the $M_V(\text{RR})$ versus $[\text{Fe}/\text{H}]$ relation. Even though paramount theoretical and observational efforts have been devoted to this long-standing problem a broad consensus on "long" and "short" distance scales has not been reached yet.

Among the different approaches discussed in the recent literature, we focus our attention on those based on the analysis of pulsation properties. These methods are attractive, since they rely on observables (period and luminosity amplitude) that are not affected by uncertainties on both distance modulus and reddening. In this context, Caputo (1997) and Caputo et al. (2000) developed a method based on the predicted PL relation for pulsators located along the first overtone blue edge (FOBE), that seems quite robust for clusters with significant numbers of *RRc* variables. According to this procedure, for each

assumption concerning the globular cluster distance modulus, one obtains the distribution of the cluster RR Lyrae stars in the M_V - $\log P$ plane. A determination of the actual distance modulus is derived by matching the observed distribution of RRc variables with the predicted relation for the FOBE (Caputo et al. 2000), i.e.

$$M_V(FOBE) = -0.685(\pm 0.027) - 2.255 \log P(FOBE) - 1.259 \log M/M_\odot + 0.058 \log Z \quad (4)$$

in such a way that no RRc variables are located in the hotter stable region.

By adopting for Carina a metallicity of $[Fe/H] = -1.7$ (i.e. $\log Z = -3.4$, see Paper II for details), we can estimate on the basis of evolutionary HB models that the mass of RRc variables is $M = 0.7M_\odot$, with an uncertainty of the order of 4% (see Bono et al. 2002). On this basis, the FOBE procedure (see Fig. 12) yields an apparent distance modulus for Carina of $DM_V = 20.19 \pm 0.04$ mag.

The distance to Carina can also be estimated using eq. (2) and by adopting $M = 0.75M_\odot$ for $RRab$ variables (Bono et al. 2002). This choice is based on the evolutionary evidence that the mass of HB models increases towards the red, i.e. when moving from RRc to $RRab$ variables. As a result, we derive $DM_V = 20.09 \pm 0.10$ mag.

Finally, eq. (3) can also be adopted to estimate the distance to Carina. In particular, by assuming $M = 0.7M_\odot$ for RRc stars and $0.75M_\odot$ for $RRab$, we obtain $DM_V = 20.19 \pm 0.12$ mag. Bearing in mind that systematic effects due to the adopted mixing-length parameter may affect the predicted PLA relation, our final estimate of the Carina distance modulus according to pulsational methods is $DM_V = 20.19 \pm 0.12$ mag. This yields $\langle M_V(RR) \rangle = 0.49 \pm 0.12$ mag that is slightly fainter than the value 0.42 ± 0.08 mag inferred from the $\langle M_V(RR) \rangle$ - $[Fe/H]$ relation given by Bono et al. (2002) for metal-poor RR Lyrae stars. On the other hand, the Bono et al. relation for $[Fe/H] = -1.5$ gives $\langle M_V(RR) \rangle = 0.50 \pm 0.09$ mag, that is slightly brighter than the estimate recently provided by Cacciari (2002), $\langle M_V(RR) \rangle = 0.57 \pm 0.04$ at $[Fe/H] = -1.5$, on the basis of several theoretical and empirical calibrations.

5. Summary and conclusions

We collected BV time series data in a region of 34×33 arcmin centered on the Carina dSph with the WFI available at the 2.2m ESO/MPI telescope. In this investigation we present some preliminary results concerning bright variables located inside the Cepheid instability strip, namely RR Lyrae and Anomalous Cepheids. The observing strategy and

the data reduction approach allowed us to identify 92 variables. Among them 75 are RR Lyrae and 15 are "bona fide" Anomalous Cepheids. We also found a field RR Lyrae and a variable located close to the Carina RGB. Current light curves when compared with those derived by SMS on the basis of photographic plates present, as expected, smooth variations over the entire pulsation cycle. Among the 75 RR Lyrae stars, 26 are new identifications, while 6 are new candidate double-mode RR Lyrae, while among the 15 Anomalous Cepheids, 7 are new identifications. Moreover, we recovered 57 out of the 140 variable sources (candidates plus "bona fide" variables) detected by SMS in the field covered by our data. However, the aperture photometry we adopted in this investigation does not allow us to assess on a firm basis the complete census of variable sources in this field. Moreover, it is worth mentioning that the current sample of bright variables is also biased toward shorter periods, since current data cover a time interval of 3 days. To overcome these problems we plan to perform PSF photometry and to merge the photometric databases collected with the 2.2m and with the CTIO 4m telescopes.

Current data concerning the pulsation properties of RR Lyrae variables disclose that they are quite similar to RR Lyrae in GGCs. Interestingly enough, we found that two objects, V158 and V182, out of the 75 variables fainter than 21.1 mag might be more massive than typical RR Lyrae stars. Their reduced periods are systematically shorter than the bulk of the RR Lyrae stars. Straightforward physical arguments based on the pulsation properties of bright variables, i.e. $V \leq 20$ mag strongly support the evidence that they are Anomalous Cepheids, i.e. He burning stars with stellar masses 2 times more massive than RR Lyrae stars. Further speculations concerning the pulsation mode, fundamental or first overtone, as well as new insights on their evolutionary history, single or binary (Bono et al. 1997a) require an accurate coverage of the light curve and detailed star count estimates of the intermediate-age main sequence stars.

We adopted three different methods to evaluate the Carina distance modulus. The FOBE method suggested by Caputo et al. (2000) provides, assuming a mean metal content of $[Fe/H]=-1.7$, an apparent distance modulus of 20.19 ± 0.04 mag, the Period-Luminosity-Amplitude relation gives, assuming mean masses of $M = 0.7M_{\odot}$ for *RRc* and $M = 0.75M_{\odot}$ for *RRab* variables, 20.09 ± 0.10 mag, while the period-luminosity-color relation supplies 20.19 ± 0.12 mag. As a whole, our distance modulus evaluation based on RR Lyrae stars is 20.19 ± 0.12 mag, and assuming a reddening correction of $E(B - V) = 0.03 \pm 0.02$ (see paper II) we derive true distance modulus of $\mu_0 = 20.10 \pm 0.12$. Distance estimates available in the literature present a large spread and depend on the adopted method. They range from $\mu_0 = 19.87$ (Mighell 1997) to $\mu_0 = 20.19 \pm 0.13$ (Dolphin 2002) according to the CMD fitting. On the other hand, Smecker-Hane et al. (1994) found $\mu_0 = 20.05 \pm 0.06$ and $\mu_0 = 20.12 \pm 0.08$ using the Tip of the RGB and the luminosity of HB stars, respectively. A

similar distance ($\mu_0 = 20.06 \pm 0.12$) was found by Mateo, Hurley-Keller, & Nemeč (1998) using the Period-Luminosity relation for dwarf Cepheids derived by McNamara (1995). The quoted authors typically assumed a mean metallicity of $[Fe/H] = -2.2 \pm 0.2$, and a mean reddening of $E(B - V) \approx 0.03 \pm 0.02$. More recently, Girardi & Salaris (2001) provided an independent distance evaluation using a new calibration of the I-band absolute magnitude of the red giant clump and the apparent I magnitude of the Carina clump derived by Udalski (1998) and for $[Fe/H] = -1.7$, $E(B - V) \approx 0.06$ they found $\mu_0 = 19.96 \pm 0.06$ mag. More accurate constraints on the Carina true distance modulus will be provided as soon as the search for variable stars will extend to fainter variables such as δ Scuti and Oscillating Blue Stragglers. The dSph galaxies that host stellar population with a wide spread in stellar ages are a fundamental laboratory to constrain the intrinsic accuracy of different groups of standard candles (Bono et al. 2002).

The data for Carina together with data for RR Lyrae variables in dSphs available in the literature support the conclusion that these stellar systems cannot be easily classified into either of the classical Oosterhoff groups. In the case of Carina, the mean period of the *RRab* variables is quite similar to the mean period of *RRab* stars in Oosterhoff type II clusters. On the other hand, the ratio between *RRc* and total number of RR Lyrae stars is typical of that seen in Oosterhoff type I globular clusters. Carina shares these characteristics with some not all of the other well-studied dSphs.

We wish to thank the referee, Dr. J. Nemeč, for several pertinent suggestions that improved the content and the readability of the paper. This work was partially supported by MURST/COFIN 2000 under the project: "Stellar Observables of Cosmological Relevance". HAS thanks the US National Science Foundation for support under the grant AST99-86943.

A. Comments on individual variables

The identification maps for the entire sample of variable stars are only available in the on-line edition of the manuscript (see Figures 13 to 20).

V10- It is located close to the spike of a bright star.

V11- It is located close to a bright star. The light curve is noisy, but it is not clear whether it is a double-mode pulsator.

V14- The light curve is mildly noisy. Possible blends with nearby faint stars.

V26- Possible double-mode pulsator.

V27- Poor-sampled light curve.

V68- The light curve is mildly noisy, possible blends with nearby faint stars.

V74- The B-band light curve is noisy. It is located close to the edge of the chip # 51.

V84- The light curve is noisy. It is located very close to a bright star.

V89- Possible double-mode pulsator.

V115- Poor-sampled light curve.

V122- Poor-sampled light curve. Possible blend with nearby faint stars.

V129- Poor-sampled light curve. It is located close to the edge of the chip # 55.

V142- It is located close to a bright star. Possible blend.

V149- Poor-sampled light curve.

V153- The light curve is noisy. Located close to a bright star.

V164- Located close to the edge of the chip # 53. Possible blend with a field galaxy.

V176- Poor-sampled light curve. It is located close to a bad column and are available 33 out of 54 measurements.

V177- Poor-sampled light curve. The star is located close to the edge of the chip # 50.

V178- Poor-sampled light curve. Located close to the edge of the chip # 51.

V180- Poor-sampled light curve.

V181- The light curve is mildly noisy. Possible blend with a faint star.

V182- Possible blend with a faint star.

V187- Poor-sampled light curve.

V190- Poor-sampled light curve.

V192- Possible double-mode pulsator or a blend with nearby faint stars.

V198- Possible double-mode pulsator.

V200- Possible blend with a faint star.

V203- Poor-sampled light curve. Possible blend with a nearby faint star.

V207- Possible double-mode pulsator.

REFERENCES

- Baade, W., & Swope, H. H. 1961, *AJ*, 66, 300
- Bersier, D., & Wood, P. R. 2002, *AJ*, 123, 840
- Bingham, E. A., Cacciari, C., Dickens, R. J., & Fusi Pecci, F. 1984, *MNRAS*, 209,765
- Bono, G., Caputo, F., Castellani, V., & Marconi, M. 1997b, *A&AS*, 121, 327
- Bono, G., Caputo, F., Castellani, V., Marconi, M., & Storm, J. 2001, *MNRAS*, 326, 1183
- Bono, G., Caputo, F., Castellani, V. Marconi, M., Storm, J. & Degl’Innocenti, S. 2002, *MNRAS*, submitted
- Bono, G., Caputo, F., Santolamazza, P., Cassisi, S., & Piersimoni, A. 1997a, *AJ*, 113, 2209
- Bono, G., Caputo, F., & Stellingwerf, R. F. 1995, *ApJS*, 99, 263
- Bono, G., Castellani, V., & Marconi, M. 2002, *ApJ*, 565, L83
- Cacciari, C. 2002, in *New Horizons in Globular Cluster Astronomy*, ed. G. Piotto, G. Meylan, G. Djorgowski, & M. Riello, (San Francisco: ASP), in press
- Caputo, F. 1997, *MNRAS*, 284, 994
- Caputo, F., Cassisi, S., Castellani, M., Marconi, G., & Santolamazza, P., 1999, *AJ*, 117, 2199
- Caputo, F., Castellani, V., Marconi, M., & Ripepi, V. 2000, *MNRAS*, 316, 819
- Caputo, F., Degl’Innocenti, S., & Marconi, M. 2002, in *Omega Centauri, A Unique Window into Astrophysics*, ed. F. van Leeuwen, J.D. Hughes, & G. Piotto (San Francisco: ASP), 185
- Carrera, R., Aparicio, A., Martinez-Delgado, D., & Alonso-Garcia, J. 2002, *AJ*, 123, 3199
- Castellani, M., Marconi, G., & Buonanno, R. 1996, *A&A*, 310, 715
- Castelli, F., Gratton, R. G., & Kurucz, R. L. 1997a, *A&A*, 318, 841
- Castelli, F., Gratton, R. G., & Kurucz, R. L. 1997b, *A&A*, 324, 432
- Corwin, T. M., Carney, B. W. 2001, *AJ*, 122, 3183
- Cox, A. N., Hodson, S. W., & Clancy, S. P. 1983, *ApJ*, 266, 94

- Cseresnjes, P. 2001, *A&A*, 375, 909
- Da Costa, G. 1988, in *IAU Symp. 126, The Harlow-Shapley Symposium on Globular Cluster Systems in Galaxies*, (Dordrecht: Kluwer), 1988, 217
- Da Costa, G. 1999, in *The Galactic Halo*, ed. B.K Gibson, T.S. Axelrod, & M.E. Putman, (San Francisco: ASP), 153
- Dolphin, A. E. 2002, *MNRAS*, 332, 91
- Gallart, C., Aparicio, A., Freedman, W., Bertelli, G., & Chiosi, C. 1999, in *The Magellanic Clouds and Other Dwarf Galaxies*, ed. T. Richtler & J.M. Braun (Aachen: Shaker Verlag)
- Girardi, L. & Salaris, M. 2001, *MNRAS*, 323, 109
- Harris, W. E. 1996, *AJ*, 112, 1487
- Held, E. V.; Clementini, G., Rizzi, L., Momany, Y., Saviane, I., & Di Fabrizio, L. 2001, *ApJ*, 562, 39
- Held, E. V., Saviane, I., Momany, Y., & Carraro, G. 2000, *ApJ*, 530, 85
- Hurley-Keller, D., Mateo, M., & Nemeč, J. M. 1998, *AJ*, 115, 1840
- Ikuta, C., & Arimoto, N. 2002, *A&A*, 391, 55
- Kaluzny, J., Kubiak, M., Szymanski, M., Udalski, A., Krzeminski, W., & Mateo, M. 1995, *A&AS*, 112, 407
- Kopacki, G. 2000, *A&A*, 358, 547
- Lavery, R. J., Seitzer, P., Walker, A. R., Suntzeff, N. B., & Da Costa, G. S. 1996, in *The Impact of Stellar Physics on Galaxy Evolution*, ed. C. Leitherer, U. Fritze-von-Alvensleben, & J. Huchra, (San Francisco: ASP), 333
- Mateo, M. 1998, *ARA&A*, 36, 435 (M98)
- Mateo, M., Fischer, P., & Krzeminski, W. 1995, *AJ*, 110, 2166
- Mateo, M., Hurley-Keller, D., & Nemeč, J. 1998, *AJ*, 115, 1856
- McNamara, D. H. 1995, *AJ*, 109, 1751
- Mighell, K. J. 1997, *AJ*, 114, 1458

- Monelli, M., et al. 2002, AJ, submitted (Paper II)
- Moore, B., Ghigna, S., Governato, F., Lake, G., Quinn, T., Stadel, J., & Tozzi, P. 1999, ApJ, 524, L19
- Nemec, J. M. 1985, AJ, 90, 204
- Nemec, J. M., Wehlau, A., & Mendes de Oliveira, C., 1988, AJ, 96, 528
- Nemec, J. M., A. F. Linnell Nemec, & Lutz, T. E. 1994, AJ, 108, 222
- Pritzl, B. J., Armandroff, T. E., Jacoby, G. H., & Da Costa, G. S. 2002, AJ, 124, 1464
- Saha, A., Monet, D. G., Seitzer, P 1986, AJ, 92, 302
- Siegel, M. H., & Majewski, S. R. 2000, AJ, 120, 284
- Silbermann, N. A., & Smith, H. A. 1995, AJ, 110, 704
- Smecker-Hane, T. A., Stetson, P. B., Hesser, J. E., & Lehnert, M. D. 1994, AJ, 108, 507
- Smecker-Hane, T. A., Stetson, P. B., Hesser, J. E., & Vandenberg, D. A. 1996, in From Stars to Galaxies: The Impact of Stellar Physics on Galaxy Evolution, ed. C. Leitherer, U. Fritze-von-Alvensleben, & J. Huchra, (San Francisco: ASP), 328
- Udalski, A. 1998, Acta Astron., 48, 113
- van Albada, T. S., & Baker, N. 1971, ApJ, 169, 311
- van den Bergh, S. 1999, A&ARv, 9, 273 (VDB)
- Walker, A. R. 1994, AJ, 108, 555
- Walker, A. R., & Nemec, J. M. 1996, AJ, 112, 2026
- Welch, D. L., & Stetson, P. B. 1993, AJ, 105, 1813

Fig. 1.— Standard deviation as a function of the instrumental b (top) and v (bottom) magnitude. Data plotted in this figure refer to chip # 51 of the frame # 46388 (b) and # 46391 (v), respectively. The exposure time of these frames is $t = 500s$, while the seeing is ≈ 0.8 arcsec.

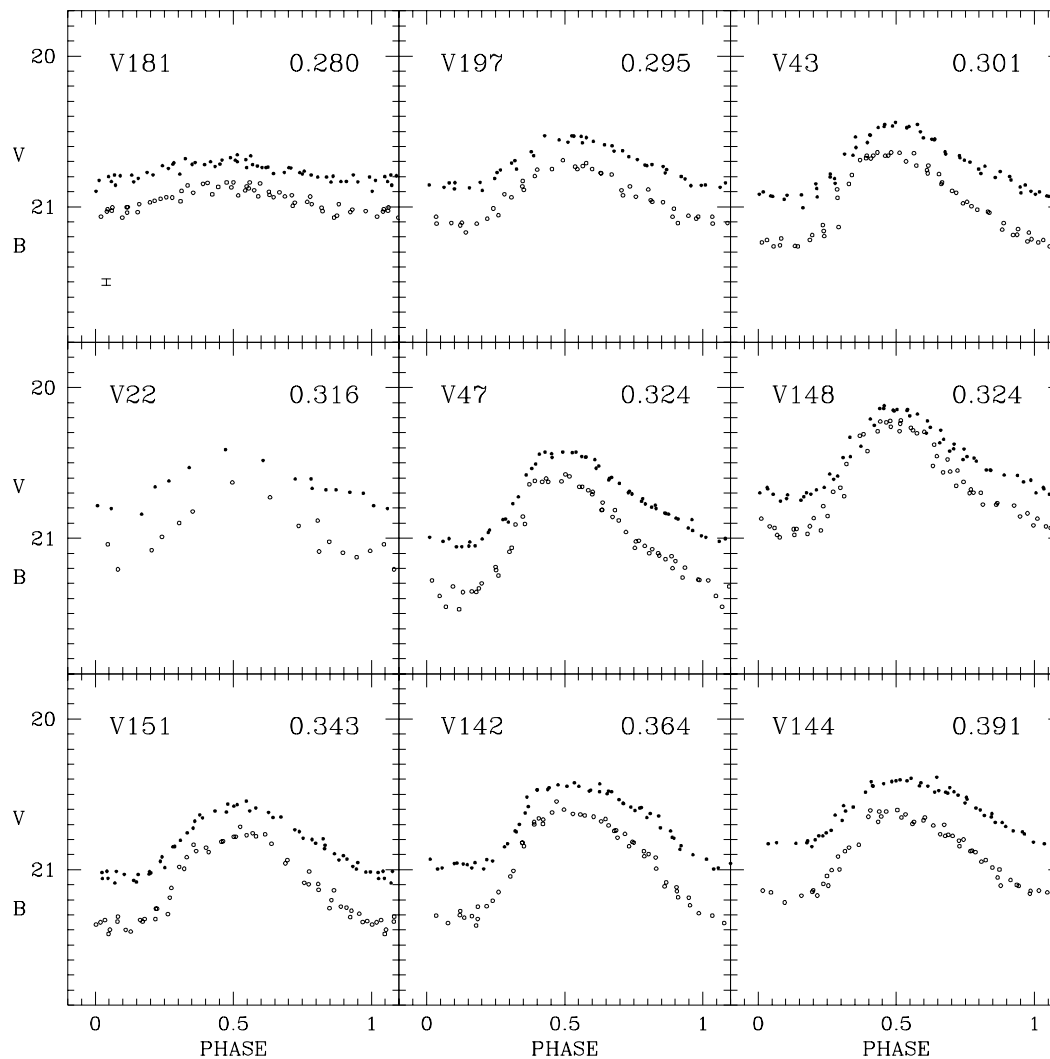


Fig. 2-a.— Light curves of fundamental and first overtone RR Lyrae detected in the central region of the Carina dSph. Filled and open squares display V and B-band light curves, respectively. In each panel are listed the identification and the period (d). The error bar shows the typical photometric uncertainty for an RR Lyrae at minimum light.

Fig. 2-b.— Continued.

Fig. 2-c.— Continued.

Fig. 2-d.— Continued.

Fig. 2-e.— Continued.

Fig. 2-f.— Continued.

Fig. 2-g.— Continued.

Fig. 2-h.— Continued.

Fig. 2-i.— Same as Fig. 2a, but the light curves refer to the suspected double-mode variables.

Fig. 2-j.— Same as Fig. 2a, but the light curves refer to Anomalous Cepheids.

Fig. 2-k.— Continued.

Fig. 2-l.— Light curve of the variable V173, located close to the Carina RGB, and of the variable V194, a possible Galactic field RR Lyrae.

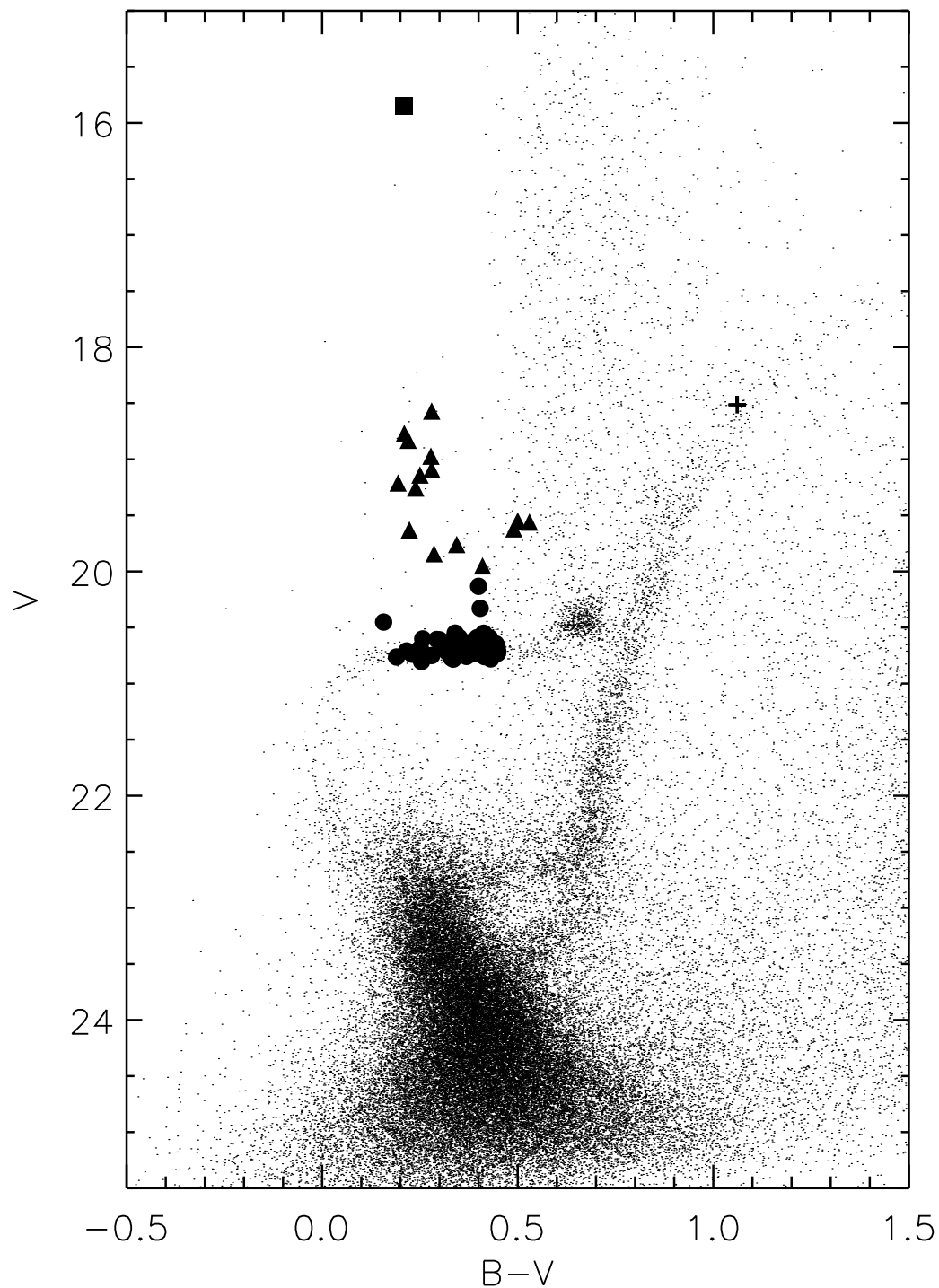


Fig. 3.— Location of the 92 identified variables in the V,B-V color-magnitude diagram. Circles and triangles mark variables fainter and brighter than $\langle V \rangle = 20$ mag respectively. Variable V173 is shown with a cross, and variable V194 with a square (see text for details).

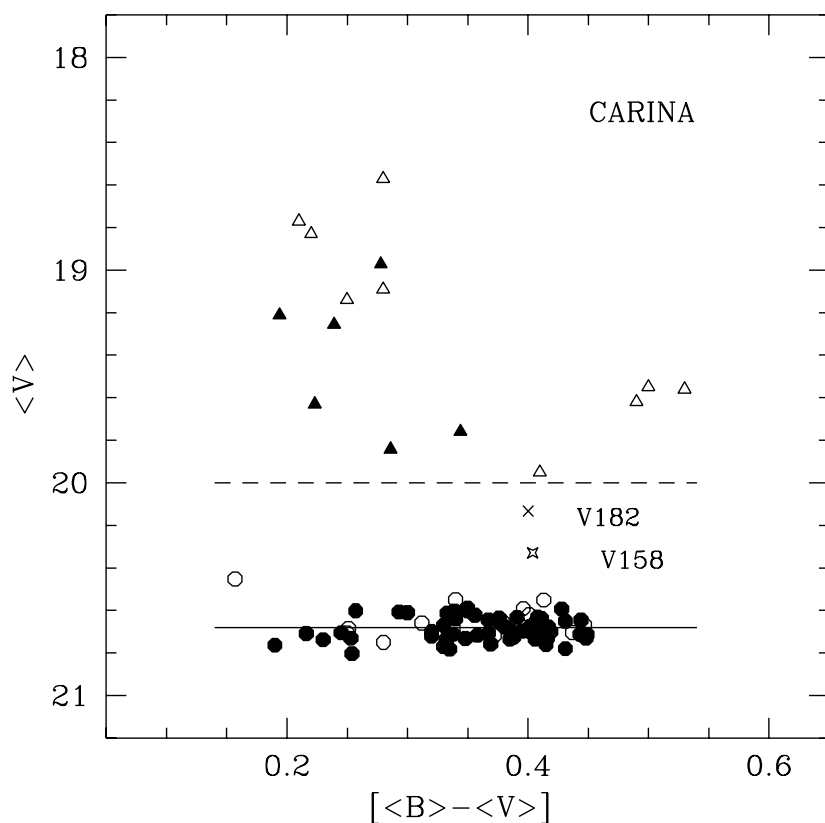


Fig. 4.— Close-up of the instability strip in the CM diagram. The symbols are the same as in Fig. 3, but variables with poorly-sampled light curves, uncertain periods, or possible blends are plotted with open symbols. The dotted line marks the edge between faint and bright variables. The variables V158 and V182 that appear significantly brighter than the mean intensity-averaged magnitude of the bulk of RR Lyrae stars ($\langle V \rangle_m = 20.68$ mag, solid line) are displayed with special symbols.

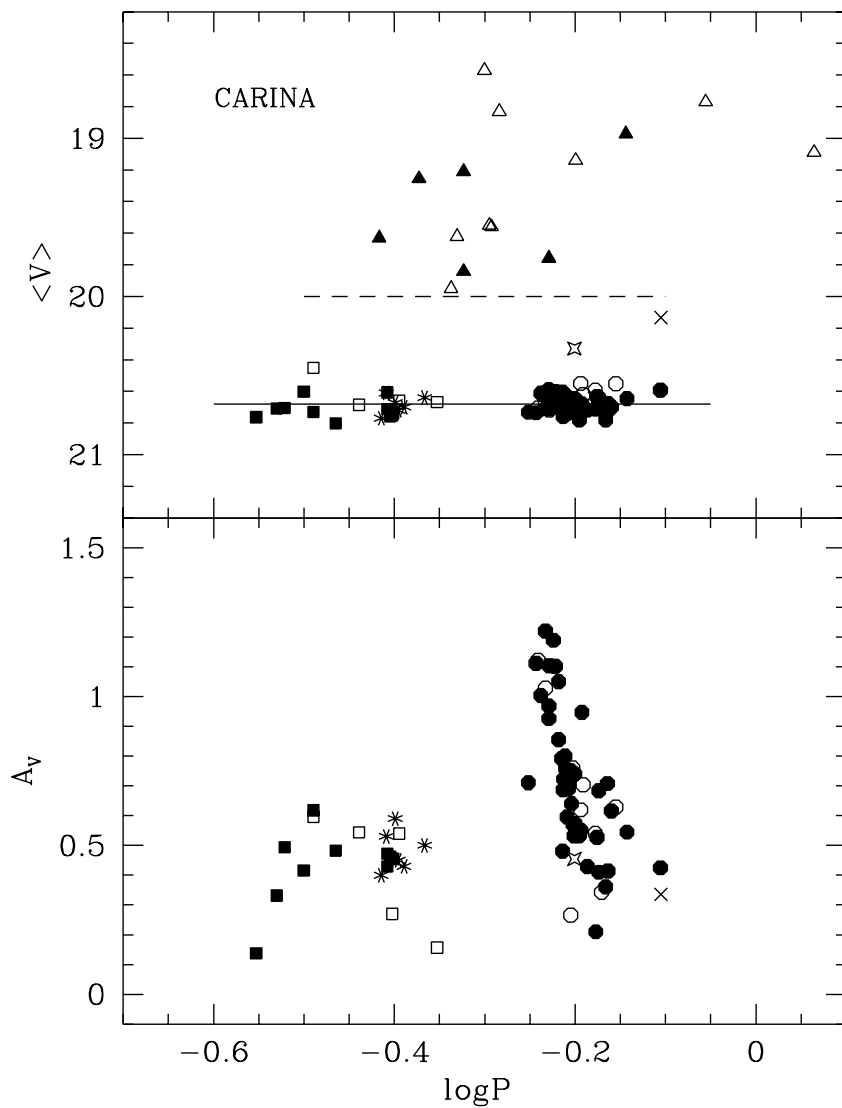


Fig. 5.— Top: Carina variables in the visual magnitude $\langle V \rangle$ vs $\log P$ plane. The gap between fundamental (circles) and first overtone (squares) variables is clearly visible. The asterisks mark the suspected double-mode pulsators. The open symbols show variables with uncertain properties. Bottom: Carina variables in the Bailey diagram, V amplitude vs $\log P$. The symbols are the same as in the top panel.

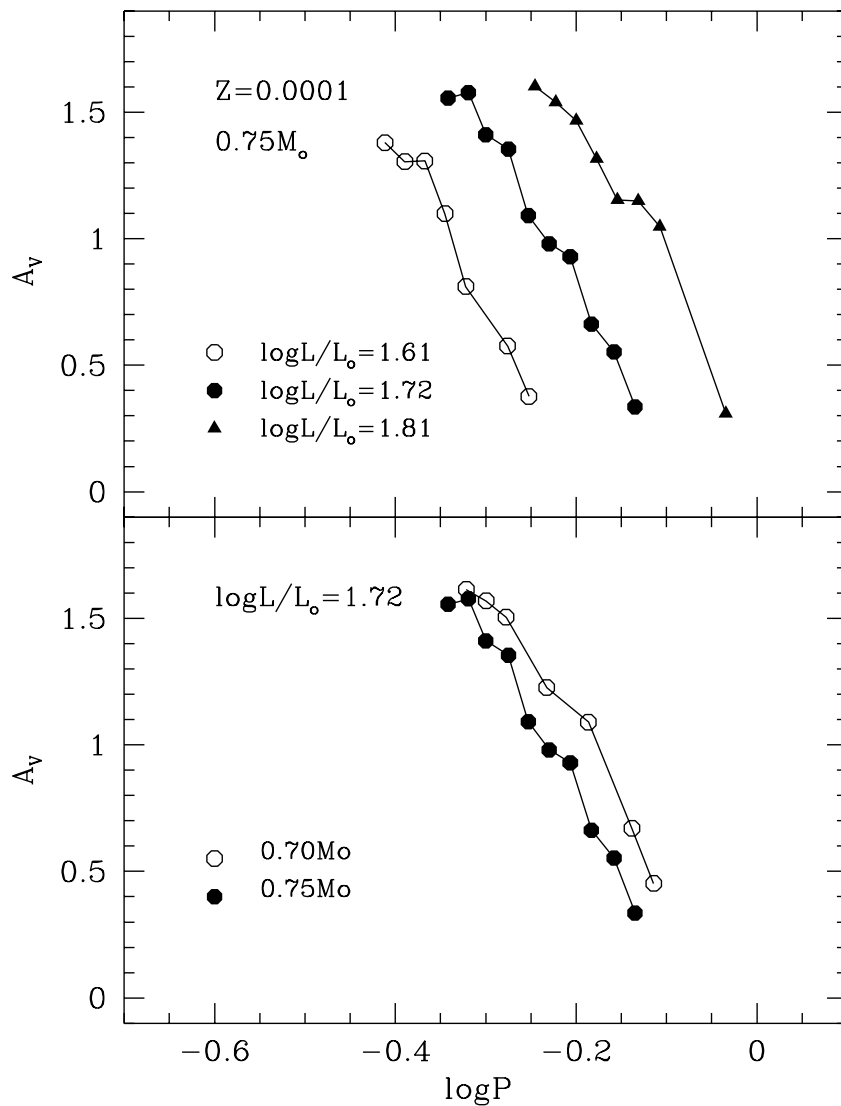


Fig. 6.— Predicted Bailey diagram, V amplitude vs $\log P$, for fundamental pulsators constructed assuming fixed stellar mass and metallicity (top panel) as well as fixed stellar luminosity and metallicity (bottom panel). Models from Di Criscienzo, Marconi & Caputo (2002).

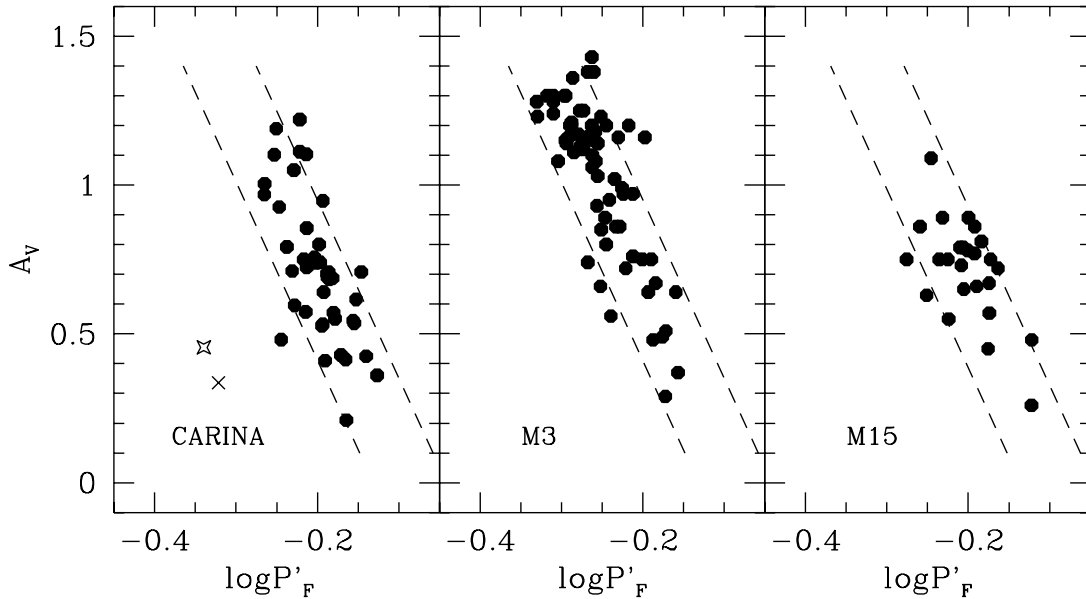


Fig. 7.— Left: ‘Reduced’ Bailey diagram A_V vs $\log P'_F$ for Carina *RRab* variables (see text for details). The dashed lines trace in this plane a ‘reduced’ period dispersion at constant amplitude, namely $\Delta \log P'_F = 0.09$. They were estimated using eq. (2) and by assuming a mass range of $0.65 - 0.80 M_\odot$. The middle and the right panel show the same data but for M3 and M15, respectively. Special symbols mark the variables, V158 (star) and V182 (cross), that show significantly shorter reduced periods. According to eq. (2), they should have masses $\approx 50\%$ larger than the bulk of the Carina *RRab* variables.

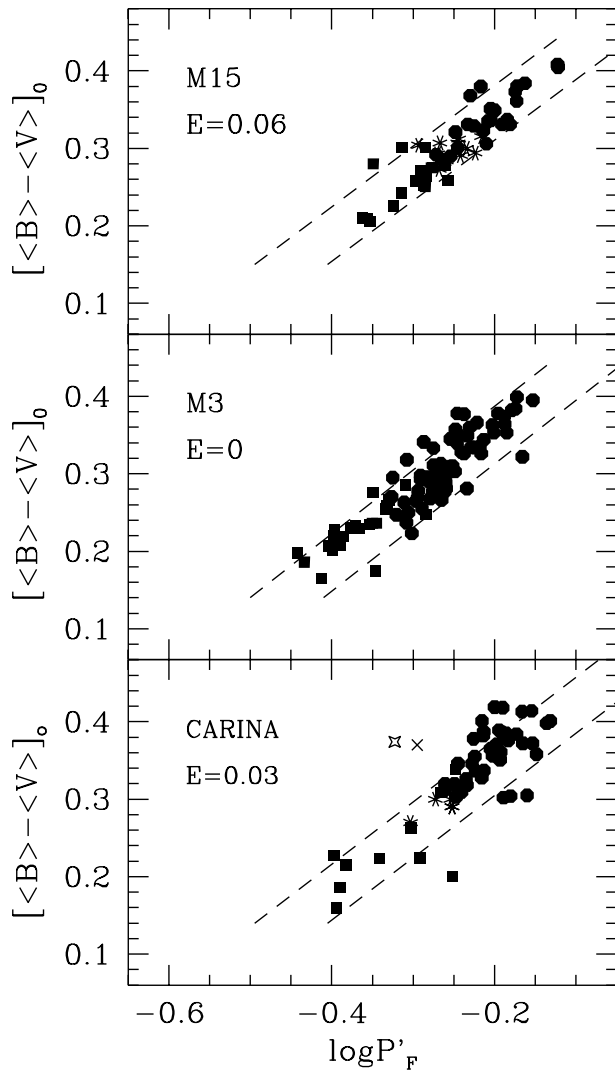


Fig. 8.— Dereddened colors vs. reduced periods for RR Lyrae stars in M15, M3, and Carina. The dashed lines depict the predicted period dispersion at constant color ($\Delta \log P'_F = 0.09$), estimated assuming stellar masses ranging from 0.65 to $0.80 M_\odot$. The present plot confirms that variables V158 (star) and V182 (cross) are significantly more massive than the bulk of Carina RR Lyrae stars (see also Fig. 7).

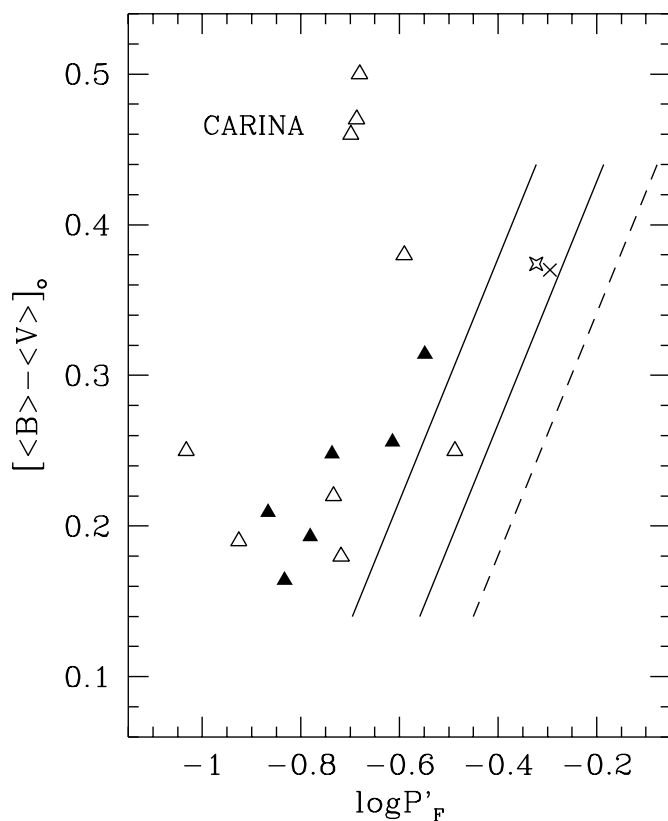


Fig. 9.— Same as Fig. 8, but for variables brighter than $\langle V \rangle = 20$ mag. The solid lines display the location in this plane of fundamental pulsators with masses 1.5 and 2 times (right to left) larger than the the bulk of RR Lyrae variables. The dashed line shows the mean locus of RR Lyrae stars. The distribution of Anomalous Cepheids show that these stars are massive pulsators. For comparison, the position of V158 and V182 are also displayed.

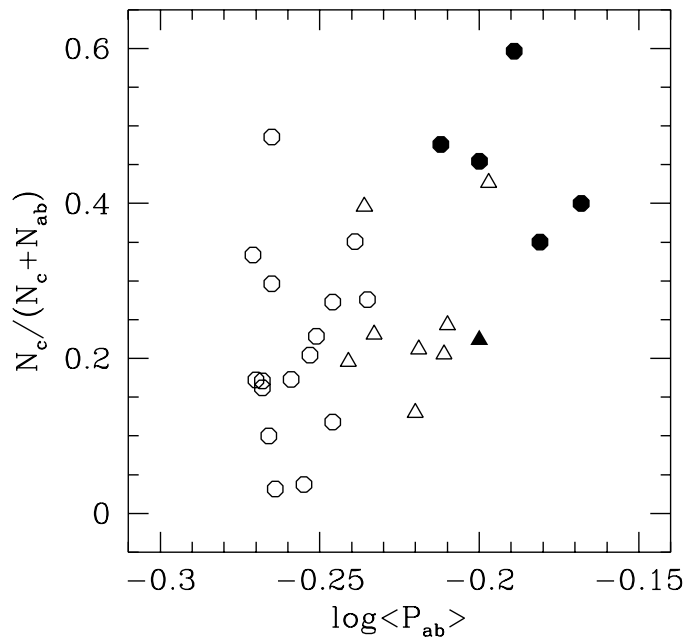


Fig. 10.— Ratio between first overtone RR Lyrae (*RRc*) and the total number of RR Lyrae as a function of the mean period of fundamental (*RRab*) variables. Filled triangle refers to Carina, filled and open circles to RR Lyrae-rich OoII and OoI globular clusters, and open triangles to dSphs (see Table 4).

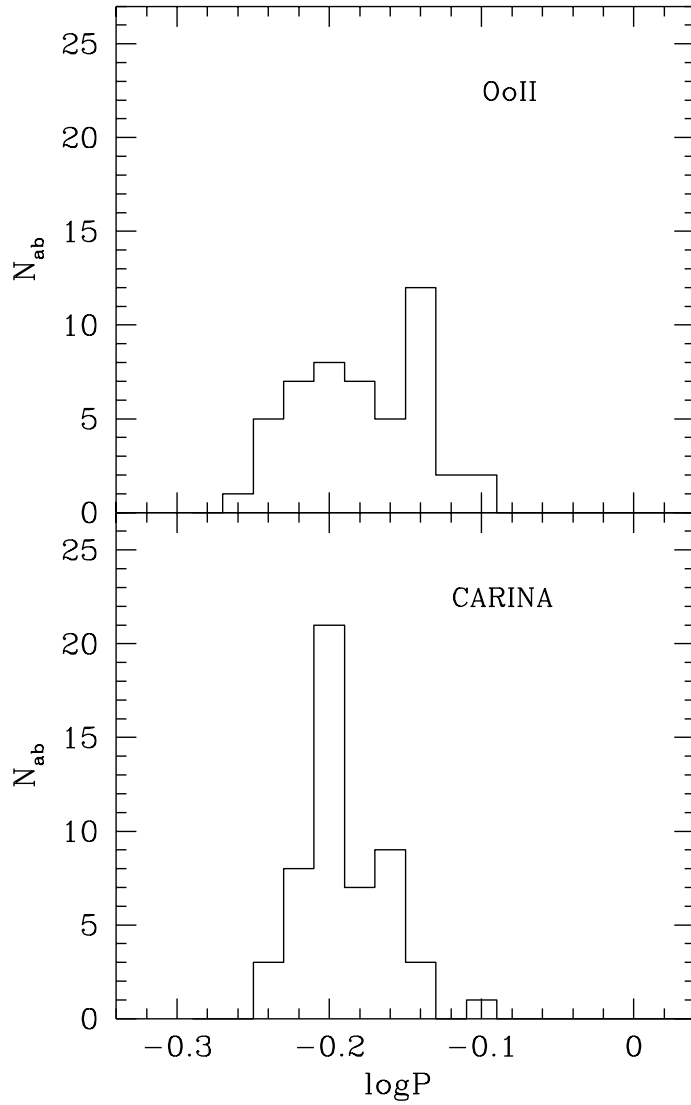


Fig. 11.— Comparison between the period distribution of the Carina *RRab* variables (bottom panel) with the cumulative distribution of *RRab* in OoII Galactic globular clusters M15, M53, and M68 (top panel).

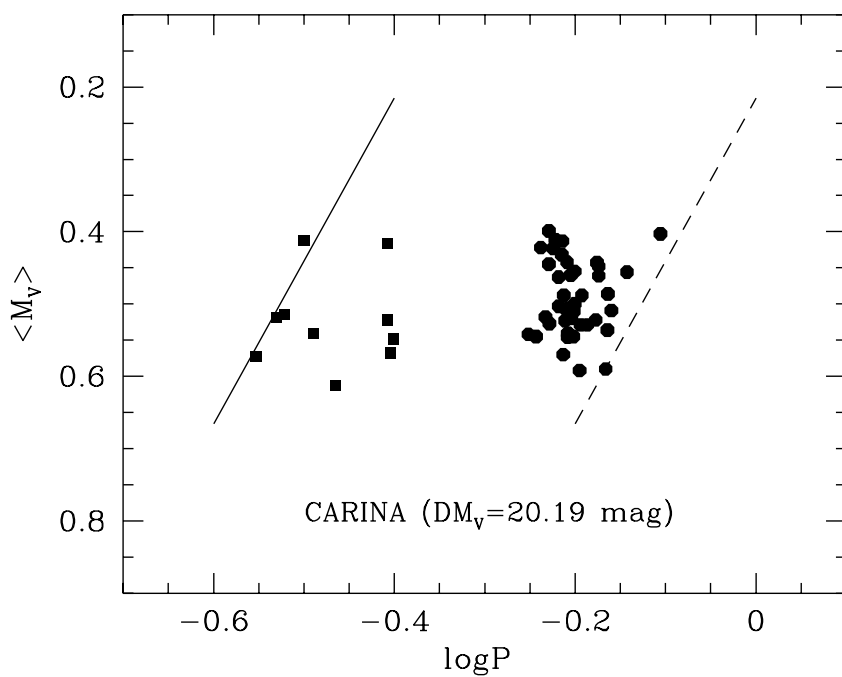


Fig. 12.— Distribution of the Carina RR Lyrae stars in the M_V - $\log P$ plane. Superimposed are the predicted blue (solid line) and red (dashed line) edge of the instability strip. By matching observed and predicted blue edge (FOBE method, Caputo et al. 2000) we estimate an apparent distance modulus for Carina of $DM_V = 20.19 \pm 0.04$ mag.

Fig. 13.— Identification map for variable stars located inside chip # 50.

Fig. 14.— Same as Fig. 13, but for chip # 51.

Fig. 15.— Same as Fig. 13, but for chip # 52.

Fig. 16.— Same as Fig. 13, but for chip # 53.

Fig. 17.— Same as Fig. 13, but for chip # 54.

Fig. 18.— Same as Fig. 13, but for chip # 55.

Fig. 19.— Same as Fig. 13, but for chip # 56.

Fig. 20.— Same as Fig. 13, but for chip # 57.